Research Article | Vol. 27, No. 2 | 21 Jan 2019 | OPTICS EXPRESS 1080
Optics EXPRESS

Polarization dependent plasmonic modes in elliptical graphene disk arrays

YUYU XIA,[1,3] YUNYUN DAI,[1,3] BO WANG,[1] ANG CHEN,[1] YANBIN ZHANG,[1] YIWEN ZHANG,[1] FANG GUAN,[1] XIAOHAN LIU,[1,2] LEI SHI,[1,2,4] AND JIAN ZI,[1,2,5]

[1]*Department of Physics, Key Laboratory of Micro-and Nano-Photonic Structures (MOE), and State Key Laboratory of Surface Physics, Fudan University, Shanghai 200433, China*
[2]*Collaborative Innovation Center of Advanced Microstructures, Nanjing 210093, China*
[3] *Y. X. and Y. D. contributed equally to this work.*
[4]*lshi@fudan.edu.cn*
[5]*jzi@fudan.edu.cn*

Abstract: Plasmonic modes at mid-infrared wavelengths in elliptical graphene disk arrays were studied. Theoretically, analytical expressions for the modes and their dependence on the size, Fermi energy and the permittivity of substrate materials of the ellipses were derived. Experimentally, the elliptical graphene disks were fabricated and their plasmonic modes were characterized with the polarization-resolved extinction spectra. Both experimental and analytical results show that two electrical dipole modes, whose dipole moments are orthogonal to each other and along the major and minor axis of the ellipse respectively, exist in the elliptical disks. By adjusting the polarization directions of the incident light, the two orthogonal plasmonic modes could be excited either together or separately, showing that the optical properties of elliptical graphene disks are highly polarization dependent. By using ultraviolet illumination to change the Fermi energy of the elliptical graphene disks, the two modes can be tuned dynamically. Moreover, the highly polarization dependent modes are able to couple with the surface phonons of the substrate, leading to polarized plasmon-phonon polaritons. Thus the elliptical graphene disks can provide more degrees of freedom to design the mid-infrared polarization-resolved photonic devices.

1. Introduction

Graphene nanostructures can support localized plasmonic resonances in the frequency range from terahertz to infrared [1–11]. The behavior of the localized plasmonic resonances depends on the size of the structure [6, 12–15], the doping level of graphene [4, 8, 9, 15, 16] and the permitivity of the substrate [17, 18]. As an example, the plasmon frequency in graphene nanostructures is proportional to the square root of Fermi energy [3, 4, 6], while inverse proportional to the square root of the corresponding length of graphene nanostructures [4, 12, 19]; the decay paths of graphene plasmons can be strongly modified by the optical phonons of the substrate [18–20],resulting in the modification of the plasmon lifetime [3]. All these unique properties make it possible in situ control the plasmons in graphene, leading to many applications [1, 2, 5, 21–23], for instance bio-sensor [24–26], THz detector [27, 28], infrared monochromatic light source [29] and modulator [30], with extensive tunabilities.

Up to now, most of the graphene plasmonic nanostructures are based on ribbon [7, 15, 18, 19, 31–35] and circular geometries [12, 13, 16]. As a result, the plasmonic resonant modes of graphene structures are either polarization independent or only available along one single polarization direction. On the other hand, elliptical geometry is inherently anisotropic [36–38]. The optical properties of a graphene ellipse could be expected to be highly polarization dependent. In this paper, theoretical and experimental investigation on the plasmonic resonances of a graphene

#349676 https://doi.org/10.1364/OE.27.001080
Journal © 2019 Received 1 Nov 2018; revised 12 Dec 2018; accepted 12 Dec 2018; published 14 Jan 2019

Optics EXPRESS

ellipse array on a substrate are presented. We found that graphene elliptical nanostructures support two plasmonic electrical dipole modes which are orthogonal to each other with dipole moments along major and minor axis of the ellipse respectively, showing polarization-dependent properties. Furthermore, it was experimentally demonstrated that the optical properties of graphene elliptical plasmonic structures can be controlled through polarization of excitation light, structure size, Fermi energy of graphene and permittivity of the substrate material etc. Compared to graphene ribbons and disks, the results obtained provide more degrees of freedom for manipulation of light-matter interactions in the mid-infrared frequency range.

2. Theoretical model

The optical conductivity and its equivalent relative dielectric constant ε_g of graphene are related with the environmental temperature, Fermi level, relaxation time and thickness of the graphene [39, 40]. In this work, temperature and thickness were considered as constant 300 K and 1 nm [41, 42] respectively. Compared with 0.33 nm or 0.24 nm thickness of graphene used by other researches [43, 44], our results are almost similar with the case of 1 nm. The Fermi level E_F, depending on the doping level of graphene, varied from 0.3 to 0.22 eV. The relaxation time τ, depending on the quality of graphene, was taken as 14 fs [6].

To theoretically characterize the polarization dependent plasmonic modes in elliptical graphene disk array, each graphene ellipse was taken as a dipole with polarizability $\widetilde{\alpha}$. The peak frequency of the imaginary part of $\widetilde{\alpha}$ corresponds to the resonant frequency of the system. And the value of that represents the extinction, which can be directly measured in experiment. In order to analytically obtain the polarizability of graphene ellipse array, each graphene ellipse is assumed as a flat ellipsoid with the length of semi-major axis a and semi-minor axis b far larger than its thickness. It is assumed the volume of such an ellipsoid V is equal to that of the ellipse, i.e. $V = 4/3\pi abc = \pi abd_g$, where c is the length of third semi-axis of the ellipsoid, and d_g is the thickness of the graphene ellipse. Therefore, $c = 3/4d_g$. Considering the non-local effect of graphene plasmons, c should be modified with an extra term Δc, $c = 3/4d_g + \Delta c$, ($\Delta c << d_g$).

To calculate the polarizability of graphene ellipsoid array, the local field in the center of each ellipsoid should be obtained. Generally, the local field is the sum of the external incident field E_{inc}, the field produced by the surrounding ellipsoids E_{sur}, and the field produced by all the image ellipsoids E_{img} when considering a substrate, $E_{\text{loc}} = E_{\text{inc}} + E_{\text{sur}} + E_{\text{img}}$. In mid-infrared frequency range, the local field on each graphene ellipsoid is assumed as a homogeneous quasi-static field.

For a single graphene ellipsoid, the local field is the external incident field, $E_{\text{loc}} = E_{\text{inc}}$. If the homogeneous quasi-static local field is along axis a(x axis) E^x_{loc} or axis b(y axis) E^y_{loc}, the induced electric field outside the ellipsoid and parallel to the local field, E^x_{ind} or E^y_{ind}, can be written as [45]

$$E^x_{\text{ind}}(x, y, z) = -E^x_{\text{loc}} \frac{\alpha_1}{V} (\widetilde{L}_1 + x \frac{\partial \widetilde{L}_1}{\partial \xi} \frac{\partial \xi}{\partial x}) \tag{1}$$

$$E^y_{\text{ind}}(x, y, z) = -E^y_{\text{loc}} \frac{\alpha_2}{V} (\widetilde{L}_2 + y \frac{\partial \widetilde{L}_2}{\partial \xi} \frac{\partial \xi}{\partial y}) \tag{2}$$

Where α_1 and α_2 are the polarizability of the ellipsoid along axis a and axis b, respectively; V is the ellipsoid volume;

$$\widetilde{L}_1 = \frac{abc}{2} \int_{\xi}^{\infty} \frac{dq}{(a^2 + q)\sqrt{(a^2 + q)(b^2 + q)(c^2 + q)}} \tag{3}$$

and

$$\widetilde{L}_2 = \frac{abc}{2} \int_{\xi}^{\infty} \frac{dq}{(b^2 + q)\sqrt{(a^2 + q)(b^2 + q)(c^2 + q)}} \tag{4}$$

Optics EXPRESS

are the modified geometrical factors along axis a and b; while ξ is one of the ellipsoidal coordinates which is determined by $\frac{x^2}{(a^2+\xi)} + \frac{y^2}{(b^2+\xi)} + \frac{z^2}{(c^2+\xi)} = 1$. [45] For simplicity, let $A_1 = \widetilde{L}_1 + x\frac{\partial \widetilde{L}_1}{\xi}\frac{\partial \xi}{\partial x}$, $A_2 = \widetilde{L}_2 + y\frac{\partial \widetilde{L}_2}{\xi}\frac{\partial \xi}{\partial y}$.

For an ellipsoid placed on an isotropic substrate with dielectric constant ε_s, as shown in Fig. 1, the influence of the substrate can be replaced by the image ellipsoid. And the local field E_{loc} of the ellipsoid at (0,0,c) is the sum of the incident field and the field produced by its image at (0,0,-c). [46]

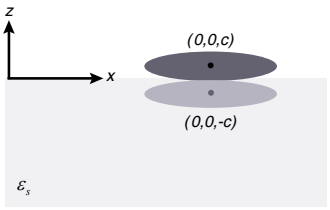

Fig. 1. The schematic diagram of a single graphene ellipsoid on an isotropic substrate with dielectric constant ε_s. Center coordinates of the ellipsoid and its image are (0,0,c) and (0,0,-c) respectively.

$$E^i_{\text{loc}} = E^i_{\text{inc}} + E^i_{\text{img}} \tag{5}$$

where $i = 1, 2$ is an index representing x and y components of the electric field respectively. According to (1), $E^i_{\text{img}}(0,0,c) = -E^i_{\text{loc}'}(0,0,-c)\frac{\alpha_i}{V}A_i(0,0,2c)$, where $E^i_{\text{loc}'}$ is the local field at the image ellipsoid (0,0,-c). The continuity boundary conditions of the electric field and electric displacement give $E^i_{\text{loc}'} = \frac{\varepsilon_0-\varepsilon_s}{\varepsilon_0+\varepsilon_s}E^i_{\text{loc}}$, thus [46].

$$E^i_{\text{img}} = -E^i_{\text{loc}}\frac{\alpha_i}{V}\frac{\varepsilon_0-\varepsilon_s}{\varepsilon_0+\varepsilon_s}A_i(0,0,2c) \tag{6}$$

where ε_0 is the vacuum dielectric constant. From (5) and (6),

$$E^i_{\text{loc}} = \frac{E^i_{\text{inc}}}{1+\frac{\alpha_i}{V}\frac{\varepsilon_0-\varepsilon_s}{\varepsilon_0+\varepsilon_s}A_i(0,0,2c)} \tag{7}$$

The dipole moment p_i of the ellipsoid is

$$p_i = \varepsilon_0\alpha_i E^i_{\text{loc}} \equiv \varepsilon_0\widetilde{\alpha}_i E^i_{\text{inc}} \tag{8}$$

where the modified polarizability $\widetilde{\alpha}_i$ is

$$\widetilde{\alpha}_i = \frac{\alpha_i}{1+\frac{\alpha_i}{V}\frac{\varepsilon_0-\varepsilon_s}{\varepsilon_0+\varepsilon_s}A_i(0,0,2c)} \tag{9}$$

For an ellipsoid array on a substrate, the local field of each ellipsoid is the sum of the field E_{inc}, E_{sur} and E_{img}. [45]

$$E^i_{\text{loc}} = E^i_{\text{inc}} + E^i_{\text{img}} + E^i_{\text{sur}} \tag{10}$$

According to (1), E^i_{sur} can be written as

$$E^i_{\text{sur}} = -E^i_{\text{loc}}\frac{\alpha_i}{V}\sum_{j\neq 0}A_i(x_j, y_j, 0) \tag{11}$$

Optics EXPRESS

According to (6), E^i_{img} can be written as

$$E^i_{\text{img}} = -E^i_{\text{loc}} \frac{\alpha_i}{V} \frac{\varepsilon_0 - \varepsilon_s}{\varepsilon_0 + \varepsilon_s} \sum A_i(x_j, y_j, 2c) \tag{12}$$

where j is an index representing different ellipses. From (10),(11) and (12), E^i_{loc} can be obtained, therefore the modified polarizability $\widetilde{\alpha}_i$ can be written as

$$\widetilde{\alpha}_i = \frac{\alpha_i}{1 + \frac{\alpha_i}{V}\beta_i} = V \frac{\varepsilon_g - \varepsilon_0}{\varepsilon_0 + (L_i + \beta_i)(\varepsilon_g - \varepsilon_0)} \tag{13}$$

where

$$L_1 = \frac{abc}{2} \int_0^\infty \frac{dq}{(a^2 + q)\sqrt{(a^2 + q)(b^2 + q)(c^2 + q)}} \tag{14}$$

and

$$L_2 = \frac{abc}{2} \int_0^\infty \frac{dq}{(b^2 + q)\sqrt{(a^2 + q)(b^2 + q)(c^2 + q)}} \tag{15}$$

are the geometrical factors along axis a and b respectively.

$$\beta_1 = \sum_{j \neq 0} A_1(x_j, y_j, 0) + \frac{\varepsilon_0 - \varepsilon_s}{\varepsilon_0 + \varepsilon_s} \sum_j A_1(x_j, y_j, 2c) \tag{16}$$

and

$$\beta_2 = \sum_{j \neq 0} A_2(x_j, y_j, 0) + \frac{\varepsilon_0 - \varepsilon_s}{\varepsilon_0 + \varepsilon_s} \sum_j A_2(x_j, y_j, 2c) \tag{17}$$

are the correction terms of L_1 and L_2 respectively.

Then the extinction cross section C_{ext} can be obtained, $C_{\text{ext}} = k \times \text{Im}[\widetilde{\alpha}_i]$ [46], and the extinction rate E_{ext} is also obtained as $E_{\text{ext}} = C_{\text{ext}}/S_{\text{period}}$, where k is the wave vector of the incident light, and S_{period} is the area of a unit cell of the ellipse array. Above results show that for each ellipsoid in the array there exist two independent polarizability $\widetilde{\alpha}_1$ and $\widetilde{\alpha}_2$ which are related to the permittivity of graphene ε_g and substrate material ε_s, therefore related to frequency, Fermi level, relaxation time τ and so on. Mathematically, by ploting $\text{Im}[\widetilde{\alpha}_1]$ and $\text{Im}[\widetilde{\alpha}_2]$ versus frequency, it can be shown that both of them exist one resonant frequency. In brief, two electrical dipole modes exist in the ellipsoid, whose dipole moments are orthogonal to each other and along the major and minor axis respectively. Many parameters including the length of major and minor axis, Fermi level of graphene and the permittivity of substrate will affect the modified polarizability, therefore the properties of the two modes.

3. Experimental results

To show the two orthogonal graphene plasmonic modes experimentally, four graphene ellipse arrays on BaF_2 with different sizes(a = 77.5 nm, b = 30 nm; a = 72.5 nm, b = 25 nm; a = 67.5 nm, b = 20 nm and a = 62.5 nm, b = 15 nm respectively.) were fabricated. For each array the period along major axis and minor axis is 200 nm and 120 nm, respectively. The fabrication process of graphene ellipse arrays is given in the method section. The schematic diagram and the SEM image of these samples are shown in Fig. 2(a). The extinction spectra $1 - T/T_0$ of the four structures were measured and shown in Figs. 2(b) and 2(c), where T and T_0 are the transmittance with and without the graphene array respectively, while the polarization

Optics EXPRESS

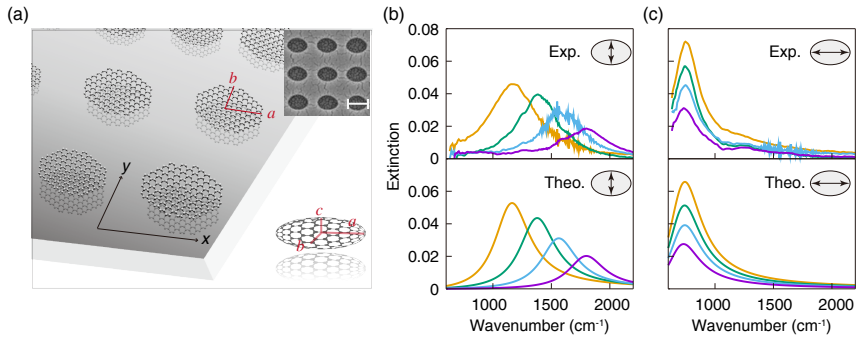

Fig. 2. (a) The schematic diagram and the SEM image of periodic graphene ellipse arrays on BaF_2. The length of semi-major axis is a, that of semi-minor axis is b, and half the length of third axis of the effective ellipsoid is c. Scale bar of the SEM image: 140 nm. (b) Experimental (upper panels) and theoretical (lower panels) extinction spectra at normal incidence with the polarization along minor axis (b) and major axis (c), respectively. From yellow line to purple line, the sizes of ellipse are: a = 77.5 nm, b = 30 nm(orange); a = 72.5 nm, b = 25 nm(green); a = 67.5 nm, b = 20 nm(blue); a = 62.5 nm, b = 15 nm(purple), respectively. In lower panel of (b) from yellow line to purple line, the extra terms Δc are: −0.07 nm, 0 nm, 0 nm, 0 nm, respectively. In lower panel of (c) from yellow to purple line, the extra terms Δc are: 0.05 nm, 0.05 nm, 0.07 nm, 0.08 nm, respectively.

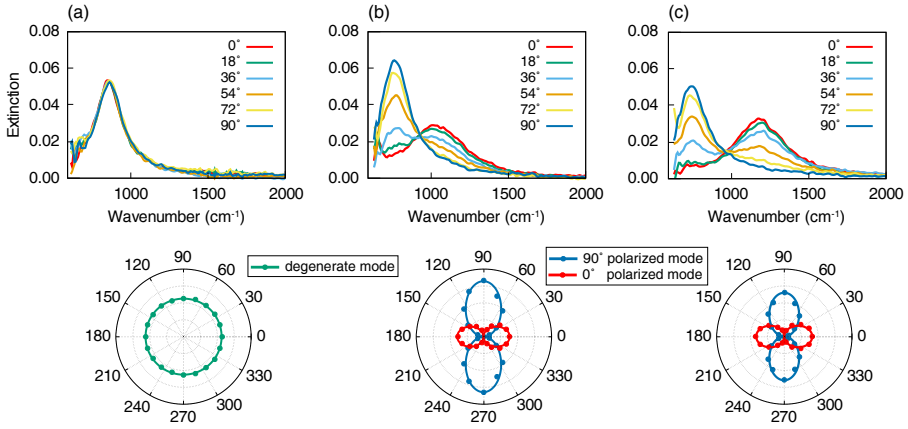

Fig. 3. Polarization-dependent extinction spectra of three different ellipticity structures. The upper panel are extinction spectra of normal incident light with polarizations varied from 0 to 90 degree. The lower panel shows extinction intensities for all polarization direction of the two resonant plasmonic modes. (a) round graphene disk with 45 nm radius. (b) Ellipse with a = 70 nm, b = 38 nm; (c) Ellipse with a = 70 nm, b = 32 nm.

direction of the incident light was set along the major and minor axis respectively. Obviously, extinction peaks are observed, corresponding to the plasmonic resonant modes. Therefore, experimental results demonstrated the existance of two eigen modes for each ellipse array. Such bimodal resonance must be due to the unique asymmetry of the ellipse. To compare the experimental results with the theoretical model, the extinction spectra are calculated, shown in the lower panel of Figs. 2(b) and 2(c). For all different array structures and polarization of the incident light along the major and minor axis of the ellipse, Fermi level E_F and relaxation time τ were properly selected as 0.34 eV and 14 fs respectively. Permittivity of BaF_2 substrate

Optics EXPRESS

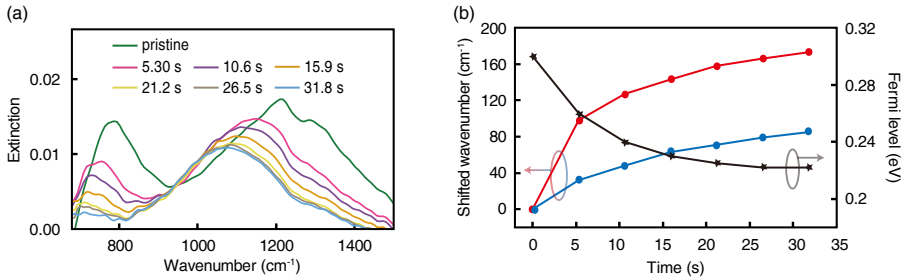

Fig. 4. (a) Redshift of the extinction spectra with illumination time. The green line shows the pristine spectrum without UV light illumination. (b) Black star line shows the variation of Fermi level with illumination time. The red dot line and the light blue dot line represent the peak shift of high-frequency and low-frequency mode, respectively.

is given in the method section. It can be seen that the theoretical extinction spectra are in good agreement with the experimental spectra both for major axis-polarization mode and minor axis-polarization mode, revealing that the plasmonic modes can be manipulated by adjusting the geometric structures of graphene to meet the specific requirements. As shown in Figs. 2(b) and 2(c), the resonant frequency of minor axis polarization mode is higher than that of major axis polarization mode. For the eigen mode that along the minor axis of the ellipse, the plasmon resonant frequency obviously shows a blueshift, while for the eigen mode that along the major axis, the resonant frequency is almost unchanged. It reveals that the resonant frequency of the mode along minor axis is more sensitive to its length.

The polarization-dependent extinction spectra were measured, shown in the upper panels of Figs. 3(b) and 3(c). The 0 degree is defined as polarization direction of the incident light along the minor axis of the ellipses and the 90 degree as the polarization direction along the major axis. It is obvious that by varying the polarization direction of normal incident light, the relative strength between the two orthogonal modes can be tuned. When the polarization direction varies from the minor axis (0 degree) to the major axis (90 degree), the high-frequency mode becomes weaker while the low-frequency mode keeps growing. The intensity of the two orthogonal resonant modes for all 360 degree polarization direction is extracted and plotted in the lower panels of Figs. 3(b) and 3(c), showing significant polarization dependence. The maximum intensity along the major axis is larger than that along the minor axis, showing the stronger light-matter interaction along major axis direction. From the polarization-dependent spectra shown in Fig. 3, it can be seen that the larger the size difference between major and minor axis is, the farther apart the two peak positions are. This approach offers good flexibility for light manipulation.

It is well known that the Fermi energy and then the optical properties of graphene can be tuned by means of applied voltage [7, 31, 32] and chemical doping via UV light [47]. Here, ultraviolet (UV) light was used. The spectra were measured with unpolarized normal incident light. As shown in Fig. 4(a), illumination of UV (355 nm) on the elliptical graphene disk array for 31.8 seconds, resulted in obvious redshift of both the two resonant peaks. This is because UV irradiation can decrease the adsorption of oxygen molecules on graphene, leading to the reduction of carrier (hole) concentration [47]. Therefore, the irradiation of ultraviolet light can continuously change the Fermi energy of graphene, leading to a redshift of the two plasmonic resonant peaks. The peak position shifts by 173 cm^{-1} for mode along the minor axis and by 85 cm^{-1} for mode along major axis. The resonant frequency of the two plasmonic modes versus illumination time of ultraviolet light is plotted in Fig. 4(b) with red dots representing high-frequency modes along minor axis and blue dots representing the low-frequency ones along major axis. By fitting the

Optics EXPRESS

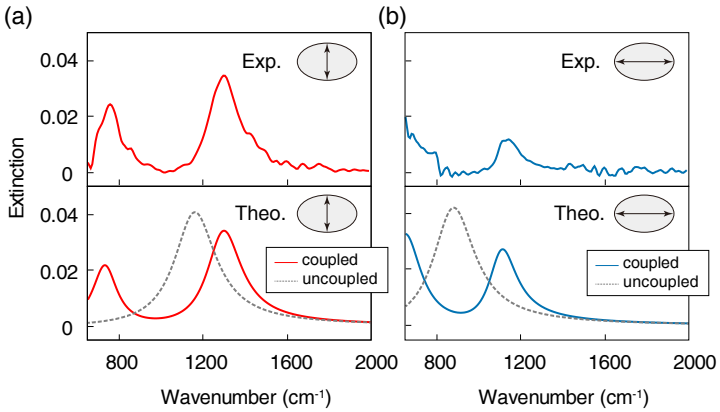

Fig. 5. Spectra measured on Si_3N_4/Si substrate and comparing the theoretical spectral with and without plsmon-phonon coupling. Upper panels: Red and blue lines are experimental extinction spectra with polarization direction of the incident light along minor and major axis respectively at normal incidence. Lower panels: Theoretical comparison of the extinction spectra with and without plsmon-phonon coupling.

two peak positions, the variation of Fermi energy with irradiation time was extracted, and shown in Fig. 4(b). The Fermi level adjusted by illumination of ultraviolet light, from the pristine 0.3 eV to 0.22 eV. With the change of Fermi energy, the resonant frequencies of two plasmonic modes will shift over a wide range. In addition, the same change of Fermi energy results in a wider tuning range for mode along major axis than that along minor axis. Therefore adjustment of E_F can dynamically tune the two plasmonic modes.

The permittivity of substrate materials will influence the plasmon resonant mode, especially the substrate of polar material with lattice vibration (phonon). Plasmons and phonons represent fundamental collective excitations in solids, and the interaction between them has fundamental implications.

In present experiment, in addition to BaF_2, polar material silicon nitride deposited on silicon (Si_3N_4/Si) was also used as substrate. Upper panels of Figs. 5(a) and 5(b) are spectra measured with polarization of incident light along minor and major axis respectively. Two distinct peaks can be clearly seen for the case along minor axis, while only one peak is observed for the incident lights polarized along the major axis. The increase of extinction with the decrease of wavenumber in low-wavenumber range indicates another peak could be beyond the measurement range. As shown in the lower panel of Figs. 5(a) and 5(b), the theoretical spectra are generally consistent with the experimental results, demonstrating that two modes are generated by the coupling of the plasmonic modes of graphene ellipse array with phonons of the substrate. As a comparison, assuming the imaginary part of the permittivity of the substrate is zero, which means no phonon exists, only one peak at 882 cm^{-1} and 1163 cm^{-1} for the two incident polarizations (grey dashed line) exists, obviously different from that with phonon coupling, as shown in the lower panel of Figs. 5(a) and 5(b). The theoretical and experimental results further demonstrate substrate materials will strongly modulate the plasmonic modes of graphene ellipse array.

4. Methods

Sample fabrications: A large-area CVD grown graphene sheet was first transferred onto a BaF_2 substrate. Graphene structures were fabricated with a 100×100 μm^2 area at the center of the graphene layer obtained by standard e-beam lithography followed by oxygen plasma etching. Fabricated samples were then exposed to Br_2 vapor for 30 seconds to increase the doping level.

Optics EXPRESS

Spectral measurements: A Bruker Vertex 70 FTIR micro-spectrometer was used for mid-infrared spectral measurements. All measurements were performed at room temperature in air. For UV illumination, a 355 nm solid-state laser was used at power density of 200 mW/cm^2.

Theoretical parameters: The permittivity of BaF_2 is

$$\varepsilon_{BaF_2} = 2.15 + \frac{0.2\lambda^2}{\lambda^2 - 29.87^2} + \frac{4.52\lambda^2}{\lambda^2 - 53.82^2}$$

wave length λ is in micron. The effective permittivity of Si3N4/Si substrate is

$$\varepsilon_{SiN}(k) = \varepsilon_{SiN\_0} + \frac{\Lambda \times k_0^2}{k_0^2 - k^2 - i \times \Gamma \times k}$$

wave number k is in cm^{-1}. $\varepsilon_{SiN\_0} = 3.8$, $\Lambda = 1.5$, $\Gamma = 100\ cm^{-1}$, $k_0 = 820\ cm^{-1}$.

5. Conclusions

In summary, the plasmonic modes of graphene ellipse array have been theoretically and experimentally investigated. Firstly, the feasibility of the theory is verified by comparing the theoretical spectra with the experimental ones. Secondly, by changing the polarized direction of normal incident light, the relative strength between the two orthogonal modes can be tuned. Thirdly, the two plasmonic modes show red shift with the increase of the axis length or decrease of the Fermi level of graphene, respectively. Finally, with a polar substrate, the coupling of graphene plasmons and substrate phonons generate two resonant modes in each axis direction of the ellipse. Our findings propose that the unique properties of anisotropic graphene structures may have many potential applications as polarization-dependent detectors, filters and sensors at infrared wavelengths.

Funding

973 and China National Key Basic Research Program (2015CB659400, 2016YFA0301100, 2016YFA0302000); National Natural Science Foundation of China (11774063, 11727811). The research of L.S. was further supported by Science and Technology Commission of Shanghai Municipality (17ZR1442300, 17142200100), State Key Laboratory of Surface Physics (ZA2014-01).

References

1. A. Grigorenko, M. Polini, and K. Novoselov, "Graphene plasmonics," Nat. Photonics **6**, 749 (2012).
2. F. Xia, H. Wang, D. Xiao, M. Dubey, and A. Ramasubramaniam, "Two-dimensional material nanophotonics," Nat. Photonics **8**, 899 (2014).
3. T. Low and P. Avouris, "Graphene plasmonics for terahertz to mid-infrared applications," ACS Nano **8**, 1086–1101 (2014).
4. F. J. García de Abajo, "Graphene plasmonics: challenges and opportunities," ACS Photonics **1**, 135–152 (2014).
5. S. Xiao, X. Zhu, B. H. Li, and N. A. Mortensen, "Graphene-plasmon polaritons: From fundamental properties to potential applications," Front. Phys. **11**, 117801 (2016).
6. F. H. Koppens, D. E. Chang, and F. J. García de Abajo, "Graphene plasmonics: a platform for strong light–matter interactions," Nano Lett. **11**, 3370–3377 (2011).
7. L. Ju, B. Geng, J. Horng, C. Girit, M. Martin, Z. Hao, H. A. Bechtel, X. Liang, A. Zettl, Y. R. Shen, and F. Wang, "Graphene plasmonics for tunable terahertz metamaterials," Nat. Nanotechnol. **6**, 630 (2011).
8. Z. Fei, A. Rodin, G. Andreev, W. Bao, A. McLeod, M. Wagner, L. Zhang, Z. Zhao, M. Thiemens, G. Dominguez, M. Thiemens, M. M. Fogler, A. H. Castro-Neto, C. N. Lau, F. Keilmann and D. N. Basov, "Gate-tuning of graphene plasmons revealed by infrared nano-imaging," Nature **487**, 82 (2012).
9. J. Chen, M. Badioli, P. Alonso-González, S. Thongrattanasiri, F. Huth, J. Osmond, M. Spasenović, A. Centeno, A. Pesquera, P. Godignon, A. Zurutuza, N. Camara, J. García de Abajo, R. Hillenbrand and F. Koppens, "Optical nano-imaging of gate-tunable graphene plasmons," Nature **487**, 77 (2012).
10. J. Christensen, A. Manjavacas, S. Thongrattanasiri, F. H. Koppens, and F. J. García de Abajo, "Graphene plasmon waveguiding and hybridization in individual and paired nanoribbons," ACS nano **6**, 431–440 (2011).

Optics EXPRESS

11. T. Zhan, X. Shi, Y. Dai, X. Liu, and J. Zi, "Transfer matrix method for optics in graphene layers," J. Physics: Condens. Matter **25**, 215301 (2013).
12. H. Yan, Z. Li, X. Li, W. Zhu, P. Avouris, and F. Xia, "Infrared spectroscopy of tunable dirac terahertz magneto-plasmons in graphene," Nano Lett. **12**, 3766–3771 (2012).
13. Z. Fang, S. Thongrattanasiri, A. Schlather, Z. Liu, L. Ma, Y. Wang, P. M. Ajayan, P. Nordlander, N. J. Halas, and F. J. García de Abajo, "Gated tunability and hybridization of localized plasmons in nanostructured graphene," ACS Nano **7**, 2388–2395 (2013).
14. X. Zhu, W. Wang, W. Yan, M. B. Larsen, P. Bøggild, T. G. Pedersen, S. Xiao, J. Zi, and N. A. Mortensen, "Plasmon–phonon coupling in large-area graphene dot and antidot arrays fabricated by nanosphere lithography," Nano Lett. **14**, 2907–2913 (2014).
15. Y. Dai, A. Chen, Y. Xia, D. Han, X. Liu, L. Shi, and J. Zi, "Symmetry breaking induced excitations of dark plasmonic modes in multilayer graphene ribbons," Opt. Express **24**, 20021–20028 (2016).
16. Z. Fang, Y. Wang, A. E. Schlather, Z. Liu, P. M. Ajayan, F. J. García de Abajo, P. Nordlander, X. Zhu, and N. J. Halas, "Active tunable absorption enhancement with graphene nanodisk arrays," Nano Lett. **14**, 299–304 (2013).
17. A. Woessner, M. B. Lundeberg, Y. Gao, A. Principi, P. Alonso-González, M. Carrega, K. Watanabe, T. Taniguchi, G. Vignale, M. Polini, J.Hone, R. Hillenbrand, and F. H. L. Koppens, "Highly confined low-loss plasmons in graphene–boron nitride heterostructures," Nat. Mater. **14**, 421 (2015).
18. V. W. Brar, M. S. Jang, M. Sherrott, S. Kim, J. J. Lopez, L. B. Kim, M. Choi, and H. Atwater, "Hybrid surface-phonon-plasmon polariton modes in graphene/monolayer h-BN heterostructures," Nano Lett. **14**, 3876–3880 (2014).
19. H. Yan, T. Low, W. Zhu, Y. Wu, M. Freitag, X. Li, F. Guinea, P. Avouris, and F. Xia, "Damping pathways of mid-infrared plasmons in graphene nanostructures," Nat. Photonics **7**, 394 (2013).
20. I. J. Luxmoore, C. H. Gan, P. Q. Liu, F. Valmorra, P. Li, J. Faist, and G. R. Nash, "Strong coupling in the far-infrared between graphene plasmons and the surface optical phonons of silicon dioxide," ACS Photonics **1**, 1151–1155 (2014).
21. F. Bonaccorso, Z. Sun, T. Hasan, and A. Ferrari, "Graphene photonics and optoelectronics," Nat. Photonics **4**, 611 (2010).
22. X. Yang, Z. Sun, T. Low, H. Hu, X. Guo, F. J. García de Abajo, P. Avouris, and Q. Dai, "Nanomaterial-based plasmon-enhanced infrared spectroscopy," Adv. Mater. **30**, 1704896 (2018).
23. A. Autere, H. Jussila, Y. Dai, Y. Wang, H. Lipsanen, and Z. Sun, "Nonlinear optics with 2D layered materials," Adv. Mater. **30**, 1705963 (2018).
24. D. Rodrigo, O. Limaj, D. Janner, D. Etezadi, F. J. G. De Abajo, V. Pruneri, and H. Altug, "Mid-infrared plasmonic biosensing with graphene," Science **349**, 165–168 (2015).
25. H. Hu, X. Yang, F. Zhai, D. Hu, R. Liu, K. Liu, Z. Sun, and Q. Dai, "Far-field nanoscale infrared spectroscopy of vibrational fingerprints of molecules with graphene plasmons," Nat. Commun. **7**, 12334 (2016).
26. Y. Li, H. Yan, D. B. Farmer, X. Meng, W. Zhu, R. M. Osgood, T. F. Heinz, and P. Avouris, "Graphene plasmon enhanced vibrational sensing of surface-adsorbed layers," Nano Lett. **14**, 1573–1577 (2014).
27. X. Cai, A. B. Sushkov, M. M. Jadidi, L. O. Nyakiti, R. L. Myers-Ward, D. K. Gaskill, T. E. Murphy, M. S. Fuhrer, and H. D. Drew, "Plasmon-enhanced terahertz photodetection in graphene," Nano Lett. **15**, 4295–4302 (2015).
28. M. M. Jadidi, A. B. Sushkov, R. L. Myers-Ward, A. K. Boyd, K. M. Daniels, D. K. Gaskill, M. S. Fuhrer, H. D. Drew, and T. E. Murphy, "Tunable terahertz hybrid metal–graphene plasmons," Nano Lett. **15**, 7099–7104 (2015).
29. V. W. Brar, M. C. Sherrott, M. S. Jang, S. Kim, L. Kim, M. Choi, L. A. Sweatlock, and H. A. Atwater, "Electronic modulation of infrared radiation in graphene plasmonic resonators," Nat. Commun. **6**, 7032 (2015).
30. S. Kim, M. S. Jang, V. W. Brar, Y. Tolstova, K. W. Mauser, and H. A. Atwater, "Electronically tunable extraordinary optical transmission in graphene plasmonic ribbons coupled to subwavelength metallic slit arrays," Nat. Commun. **7**, 12323 (2016).
31. H. Hu, F. Zhai, D. Hu, Z. Li, B. Bai, X. Yang, and Q. Dai, "Broadly tunable graphene plasmons using an ion-gel top gate with low control voltage," Nanoscale **7**, 19493–19500 (2015).
32. V. W. Brar, M. S. Jang, M. Sherrott, J. J. Lopez, and H. A. Atwater, "Highly confined tunable mid-infrared plasmonics in graphene nanoresonators," Nano Lett. **13**, 2541–2547 (2013).
33. X. Shi, D. Han, Y. Dai, Z. Yu, Y. Sun, H. Chen, X. Liu, and J. Zi, "Plasmonic analog of electromagnetically induced transparency in nanostructure graphene," Opt. Express **21**, 28438–28443 (2013).
34. D. B. Farmer, D. Rodrigo, T. Low, and P. Avouris, "Plasmon–plasmon hybridization and bandwidth enhancement in nanostructured graphene," Nano Lett. **15**, 2582–2587 (2015).
35. Z. Fei, M. Goldflam, J. S. Wu, S. Dai, M. Wagner, A. McLeod, M. Liu, K. Post, S. Zhu, G. Janssen, M. M. Fogler, and D. N. Basov, "Edge and surface plasmons in graphene nanoribbons," Nano Lett. **15**, 8271–8276 (2015).
36. J. Chen, Y. Zeng, X. Xu, X. Chen, Z. Zhou, P. Shi, Z. Yi, X. Ye, S. Xiao, and Y. Yi, "Plasmonic absorption enhancement in elliptical graphene arrays," Nanomaterials **8**, 175 (2018).
37. E. Mobini, A. Rahimzadegan, R. Alaee, and C. Rockstuhl, "Optical alignment of oval graphene flakes," Opt. Lett. **42**, 1039 (2017).
38. R. Yu, L. M. Liz-Marzán and F. J. García de Abajo, "Universal analytical modeling of plasmonic nanoparticles," TUTORIAL REVIEW **8**, 175 (2018).
39. B. Wunsch, T. Stauber, F. Sols, and F. Guinea, "Dynamical polarization of graphene at finite doping," New J. Phys. **8**, 318 (2006).

Optics EXPRESS

40. E. Hwang and S. D. Sarma, "Dielectric function, screening, and plasmons in two-dimensional graphene," Phys. Rev. B **75**, 205418 (2007).
41. B. Wang, X. Zhang, X. Yuan, and J. Teng, "Optical coupling of surface plasmons between graphene sheets," Appl. Phys. Lett. **100**, 131111 (2012).
42. X. Guo, H. Hu, B. Liao, X. Zhu, X. Yang, and Q. Dai "Perfect-absorption graphene metamaterials for surface-enhanced molecular fingerprint spectroscopy," Nanotechnology **29**, 184004 (2018).
43. K. J. A. Ooi and D. T. Tan, "Nonlineargraphene plasmonics"Proc.R.Soc.A **473**, 20170433 (2017).
44. S. de Vega and F. J. García de Abajo, "Plasmon Generation through Electron Tunneling in Graphene"ACS Photonics **4**, 2367 (2017).
45. C. F. Bohren and D. R. Huffman, *Absorption and scattering of light by small particles* (John Wiley & Sons, 2008).
46. J. D. Jackson, *Classical electrodynamics* (John Wiley & Sons, 2012).
47. Y. Dai, Y. Xia, T. Jiang, A. Chen, Y. Zhang, Y. Bai, G. Du, F. Guan, S. Wu, X. Liu, L. Shi, and J. Zi, "Dynamical tuning of graphene plasmonic resonances by ultraviolet illuminations," Adv. Opt. Mater. **6**, 1701081 (2018).